THE JOURNAL OF PHYSICAL CHEMISTRY B

Article

pubs.acs.org/JPCB

Heterogeneous Slow Dynamics of Imidazolium-Based Ionic Liquids Studied by Neutron Spin Echo

Maiko Kofu,[†] Michihiro Nagao,[‡,§] Takeshi Ueki,[∥] Yuzo Kitazawa,[∥] Yutaro Nakamura,[∥] Syota Sawamura,[∥] Masayoshi Watanabe,[∥] and Osamu Yamamuro*[,†]

[†]Institute for Solid State Physics, University of Tokyo, 5-1-5 Kashiwanoha, Kashiwa, Chiba 277-8581, Japan

[‡]NIST Center for Neutron Research, National Institute of Standards and Technology, 100 Bureau Drive, Gaithersburg, Maryland 20899-6102, United States

[§]Center for Exploration of Energy and Matter, Indiana University, Bloomington, Indiana 47408-1398, United States

[∥]Department of Chemistry and Biotechnology, Yokohama National University, 79-5 Tokiwadai, Hodogaya-ku, Yokohama, Kanagawa 240-8501, Japan

ABSTRACT: We have investigated structure and relaxation phenomena for ionic liquids 1-octyl-3-methylimidazolium hexafluorophosphate ($C8mimPF_6$) and bis-(trifluoromethylsulfonyl)imide (C8mimTFSI) by means of neutron diffraction and neutron spin echo (NSE) techniques. The diffraction patterns show two distinct peaks appeared at scattering vectors Q of 0.3 and 1.0 Å^{-1}. The former originates from the nanoscale structure characteristic to ionic liquids and the latter due to the interionic correlations. Interestingly, the intensity of the low-Q peak drastically grows upon cooling and keeps growing even below the glass transition temperature. The NSE measurements have been performed at these two Q positions, to explore the time evolution of each correlation. The relaxation related to the ionic correlation (ionic diffusion) is of Arrhenius-type and exhibits nonexponential behavior. The activation energy (E_a) of the ionic diffusion, which is linked to viscosity, depends on the type of anion; the larger is the anion size, the smaller E_a becomes for most of anions. On the other hand, two kinds of relaxation processes, slower and faster ones, are found at the low-Q peak position. The most significant finding is that the fraction of the slower relaxation increases and that of the faster one decreases upon cooling. Combining the NSE data with the diffraction data, we conclude that there exist two parts in ILs: one with the ordered nanostructure exhibiting the slow relaxation, and the other with disordered structure showing faster relaxation. The structure and dynamics of ILs are heterogeneous in nature, and the fraction of each part changes with temperature.

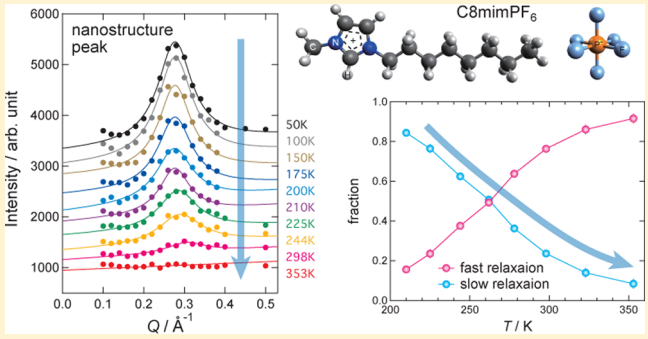

INTRODUCTION

A series of organic ionic compounds have melting temperatures lower than room temperature despite the existence of their strong and long-range Coulomb interaction. These compounds are called "room temperature ionic liquids (RTILs)" or simply "ionic liquids (ILs)". Their chemical structures include bulky cations, such as alkylimidazolium, alkylprydinium, alkylammonium, etc., which consist of positively charged core parts and hydrophobic alkyl chains. On the other hand, halogens (Cl^-, Br^-, I^-) and various ionic groups, for example, NO_3^-, BF_4^-, PF_6^-, $(CF_3SO_2)_2N^-$, can be the anions of ILs. ILs are remarked as novel green solvents and electrochemical materials with negligible vapor pressure and combustibility. Their physicochemical properties are controlled by choosing cations and/or anions, so that ILs have been remarked as designers liquids with a variety of applications.

Recently, the basic scientific studies on ILs are in great progress as well as application studies. In particular, a lot of structural information has been accumulated by X-ray/neutron scattering[1−12] and computer simulation studies.[7,8,13,14] One of the important issues in ILs is the origin of a peak appeared around Q = 0.3 Å^{-1}, which was first discovered by Triolo et al.[3] This peak is often called "prepeak" or "domain peak", but in this Article we use the term "low-Q peak" so as not to specify any predefined meaning. The correlation distance corresponding to the Q value is roughly proportional to $2n$ Å (n: alkyl carbon number) and is almost independent of the type of anions.[3,4] There seems to be a consensus that the distance roughly corresponds to the distance between two polar entities (core part of cation or anion) separated by nonpolar entities (alkyl chains). The question arises as to what kind of three-dimensional arrangement of the structure is realized in ILs. So far, several types of structural model have been proposed, for instance, pseudomicellar structure, lamellar-like structure, alkyl-group channels, etc. The details of the arrangement are,

Received: December 21, 2012
Published: February 7, 2013

   dx.doi.org/10.1021/jp312608r | J. Phys. Chem. B 2013, 117, 2773−2781

however, still controversial. In this Article, we tentatively call this structure "nanostructure".

In terms of dynamics in ILs, microscopic motions have been investigated by nuclear magnetic resonance (NMR)[15−19] and quasielastic neutron scattering (QENS)[20−24] measurements, while macroscopic features have been proved by viscoelastic,[25−27] dielectric,[28−30] and ionic conductivity[16,26,31,32] measurements. Among these measurement methods, QENS is the most powerful tool to investigate microscopic dynamics in the time domain from 1 ps to 10 ns and the space range from 1 to 100 Å. Another merit of QENS is that either coherent or incoherent scattering can be dominant by selective deuteration; $\sigma_{coh}(H) = 1.76$ barn, $\sigma_{inc}(H) = 80.27$ barn, $\sigma_{coh}(D) = 5.59$ barn, and $\sigma_{inc}(D) = 2.05$ barn, where σ is a neutron scattering cross section. The coherent neutron scattering allows us to explore the specific collective dynamics with a finite length scale by choosing the scattering vector Q. On the other hand, the incoherent neutron scattering gives us the information on the self-motions. The incoherent QENS studied by Triolo et al.[20,21] demonstrated that a Q- and T-insensitive fast (subps) relaxation and a non-Debye and non-Arrhenius slow relaxation are present as in the case of glass-forming molecular liquids. Recent coherent neutron spin echo (NSE) works with deuterated ILs, 1-hexyl-3-methylimidazolium hexafluorophosphate (d-C6mimPF$_6$)[23] and 1-octyl-3-methylimidazolium chloride (d-C8mimCl),[24] also demonstrated the non-Debye nature of the ionic motions but could not show a clear relaxation of the nanostructure at the low-Q peak position in a nanosecond time range.

In this Article, we have investigated the relaxation of the nanostructure at the low-Q peak and the ionic motions in 1-octyl-3-methylimidazolium hexafluorophosphate (C8mimPF$_6$) and 1-octyl-3-methylimidazolium bis(trifluoromethylsulfonyl)-imide (C8mimTFSI) using NSE. Our previous NSE work on C8mimCl[24] indicates that the relaxation time of the nanostructure is longer than 100 ns, which is difficult to be observed even by NSE measurements. The viscosity of ILs changes with the type of anion; when the alkyl carbon number is fixed to 8, the viscosity follows the order [Cl] > [NO$_3$] > [PF$_6$] > [CF$_3$SO$_3$] > [TFSI].[25,26] It is expected that the relaxation of the nanostructure (and the ionic diffusion) in C8mimPF$_6$ or C8mimTFSI can become faster than that in C8mimCl. Therefore, we have focused on C8mimPF$_6$ and C8mimTFSI in this work and have actually succeeded to observe the slow relaxation of the nanostructure. The chemical structures of ILs are shown in Figure 1. This is the first detailed study on the dynamics associated with the nanostructure corresponding to the low-Q peak. Because the alkyl chain is fixed to octyl (C8) in these three samples, anion dependence of the relaxation can also be investigated.

EXPERIMENTAL SECTION

Sample Preparation. 1-Methylimidazole-d_6 (98% atom D) and 1-bromooctane-d_{17} (98% atom D) were purchased from CDN isotope. D$_2$O and CDCl$_3$ were from Sigma-Aldrich. LiTFSI was from Kishida Chemical. All other chemical reagents were from Wako. All chemical reagents were used as received without further purification. (Certain commercial materials are identified in this Article to foster understanding. Such identification does not imply recommendation or endorsement by the National Institute of Standards and Technology, nor does it imply that the materials identified are necessarily the best available for the purpose.)

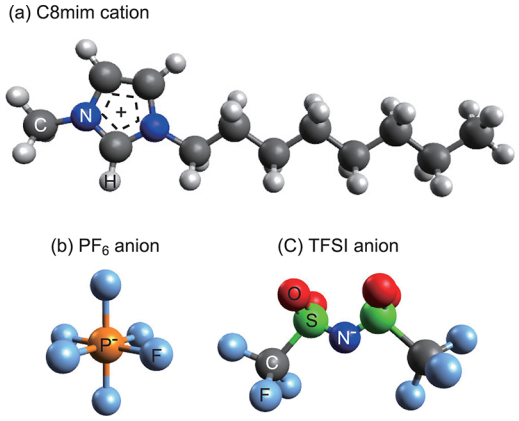

Figure 1. Chemical structures of (a) C8mim ($C_{12}H_{23}N_2$) cation, (b) PF_6 anion, and (c) TFSI ($[CF_3SO_2]_2N$) anion.

C8mimTFSI and C8mimPF$_6$ were prepared following the procedure reported earlier[33,34] with a slight modification. 1-Methyl-3-octyl imidazolium bromide (C8mimBr) was first prepared by the quaternization reaction. 1-Methylimidazole-d_6 (87.7 mL, 90.7 mmol) was slowly added dropwise to a slight excess of 1-bromooctane-d_{17} (16.4 mL, 95 mmol) toluene solution in a two-neck round-bottom flask at room temperature. After the flask mixture was stirred for a week at room temperature, unreacted 1-bromooctane-d_{17} was removed by evaporation. The resulting white powder was dissolved in CDCl$_3$ and then washed with a large amount of D$_2$O. The white crystal was dried under reduced pressure (19.2 g, 64.3 mmol, yield = 70.9%). C8mimTFSI was prepared by metathesis of C8mimBr (7.35 g, 24.6 mmol) with LiTFSI (8.55 g, 29.8 mmol) in D$_2$O and purified by washing with a large amount of D$_2$O stirring for a week. The halide content was checked by addition of AgNO$_3$ (9.05 g, 23.1 mmol, yield = 94%). C8mimPF$_6$ was prepared by a manner similar to that of C8mimTFSI, except NaPF$_6$ was used for the metathesis of C8mimBr, instead of using LiTFSI. C8mimPF$_6$ was also yielded quantitatively. C8mimTFSI and C8mimPF$_6$ were finally dried under reduced pressure at 80 °C for 48 h prior to use.

Neutron Scattering Measurements. Polarized neutron diffraction and neutron spin echo experiments were performed using the NG5-NSE spectrometer[35,36] at the NIST Center for Neutron Research (NCNR) of National Institute of Standards and Technology (NIST, USA). The spectrometer is installed at the NG5 of the guide hall at the NCNR. The beamline includes a neutron velocity selector to choose a neutron wavelength and a transmission polarizer and a reflection analyzer for the capability of neutron polarization analyses. The wavelength of used neutrons was 6 Å with the wavelength resolution of about 20%. The diffraction patterns were collected in the Q range from 0.1 to 1.4 Å^{-1} for all samples. As for the samples of C8mimPF$_6$ and C8mimCl, the temperature evolution of the diffraction peaks was investigated at the temperature between 50 and 300 K. The spin echo measurements were carried out at the diffraction peak positions, 0.28 and 1.0 Å^{-1} for C8mimPF$_6$, and 0.29 and 0.8 Å^{-1} for C8mimTFSI. The data were collected at temperatures ranging from 225 to 353 K and at Fourier times between 0.007 and 17.5 ns to observe the collective movements at the corresponding correlation peaks. The resolution data were taken at 50 K for each Q. The temperature was controlled with a closed cycle refrigerator. The DAVE software package

dx.doi.org/10.1021/jp312608r | J. Phys. Chem. B 2013, 117, 2773−2781

was used to reduce the NSE data from the echo signal to the intermediate scattering function.[37]

Polarization Analyses. The polarization analysis enables us to separate experimentally the coherent and incoherent nuclear scattering. For the sample with randomly oriented nuclei spins, nonspin flip scattering originates from coherent scattering and 1/3 of incoherent scattering, while spin flip scattering only from 2/3 of incoherent scattering:

$$I_{NSF} = I_{coh} + \frac{1}{3} I_{inc} \quad (1)$$

$$I_{SF} = \frac{2}{3} I_{inc} \quad (2)$$

For NSE measurements, the intermediate scattering function, $I(Q,t)$, can be ideally written by

$$I(Q, t) \propto \frac{A}{I_{NSF} - I_{SF}} \quad (3)$$

where A is the amplitude of the echo signal, and I_{NSF} and I_{SF} are the nonspin-flip and spin-flip scattered intensities.

RESULTS AND DISCUSSION

Neutron Diffraction. We have investigated diffraction patterns of C8mimX (X = Cl, PF_6, TFSI) by using the neutron spin echo instrument. Figure 2 shows the coherent scattering

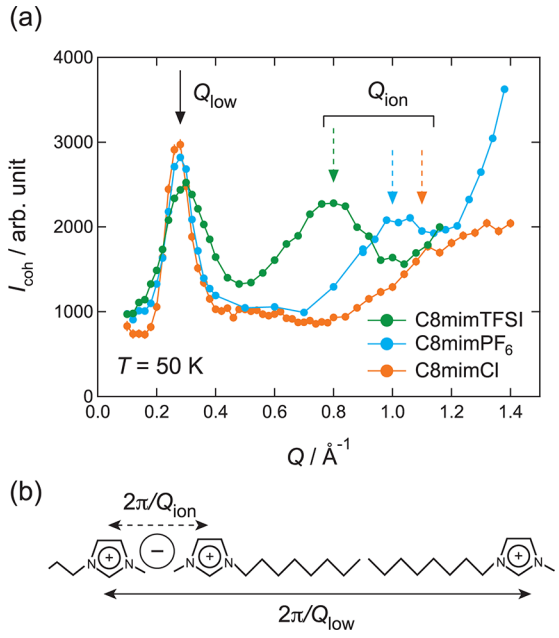

Figure 2. (a) Coherent scattering intensity as a function of Q at T = 50 K for C8mimX (X = TFSI, PF_6, Cl). The arrows denote the Q positions (Q_{low} and Q_{ion}) at which NSE measurements were performed. Error bars throughout this Article represent one standard deviation, which is often smaller than the symbols in the plot. (b) Schematic drawing of the correlations between the imidazolium rings.

measured as a function of Q at 50 K for all three samples. Background scattering from the empty can was subtracted from the data taking the sample transmission into consideration.

Two distinct diffraction peaks were observed at Q = 0.28 and 1.1 Å^{-1} for C8mimCl, at Q = 0.28 and 1.0 Å^{-1} for C8mimPF$_6$, and at Q = 0.29 and 0.8 Å^{-1} for C8mimTFSI. The peak at $Q \approx$ 0.3 Å^{-1} (=Q_{low}) is the "low-Q peak" mentioned in the Introduction. The two polar groups (imidazolium rings or anions) are separated by the alkyl chains, and the characteristic distance, $2\pi/Q_{low}$, corresponds to a repeating unit of the ordering between polar and nonpolar entities. On the other hand, the peaks at Q_{ion} (0.8 Å^{-1} < Q_{ion} < 1.1 Å^{-1}) are assigned to the correlation between adjacent polar groups not separated by the alkyl chain (see Figure 2b), reflecting the charge ordering. This is justified by the fact that this peak shifts toward lower Q with increasing anion size (ionic radius; r(Cl) < r(PF_6) < r(TFSI)).

The neutron diffraction data were also collected at temperatures higher than 50 K. Figure 3 shows temperature

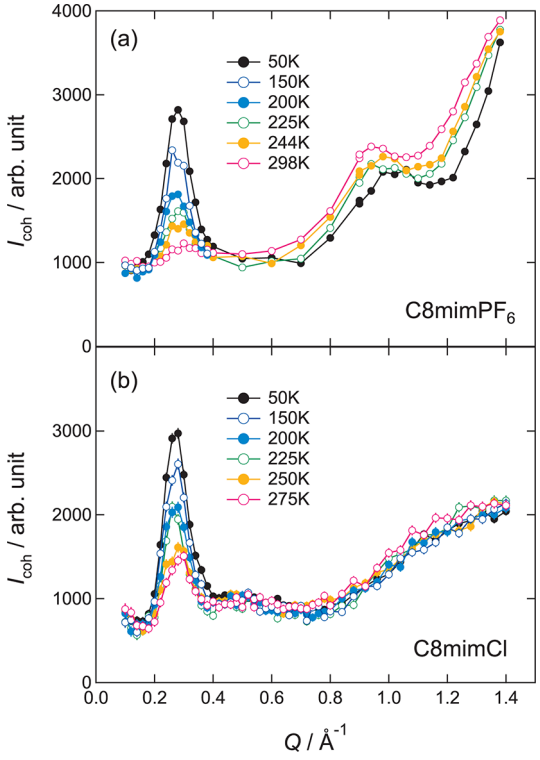

Figure 3. Temperature dependence of diffraction patterns for (a) C8mimPF$_6$ and (b) C8mimCl.

dependence of the diffraction patterns of C8mimX (X = PF_6, Cl). The peak position for the ionic correlation (Q_{ion}) shifts toward lower Q upon heating. This phenomenon is associated with the change of mass density. Similar results were obtained for C4mimPF$_6$,[2] ammonium-based IL,[11] and pyrrolidinium-based ILs.[12] On the other hand, the Q_{ion} in C8mimCl was insensitive to temperature, as reported in the previous study.[24] This fact is probably attributed to the stronger charge ordering in C8mimCl; a Cl ion is sandwiched between two imidazolium rings.[1] Interestingly, the low-Q peak becomes more pronounced on cooling. To obtain quantitative information about the temperature dependence of the low-Q peak, the peak was fitted to a Lorentz function as follows:

$$I(Q) = I_{low} \frac{1}{\pi} \frac{\Gamma}{(Q - Q_{low})^2 + \Gamma^2} + I_0(Q) \quad (4)$$

where I_{low} is the integrated intensity of the peak, Q_{low} represents the peak position, Γ denotes the half-width at half-maximum (HWHM), and $I_0(Q)$ is the coherent scattering, which does not exhibit a clear peak shape and was assumed to be a linear

dx.doi.org/10.1021/jp312608r | J. Phys. Chem. B 2013, 117, 2773−2781

function of Q in the fitting. The peak profiles were fitted well as shown in Figure 4.

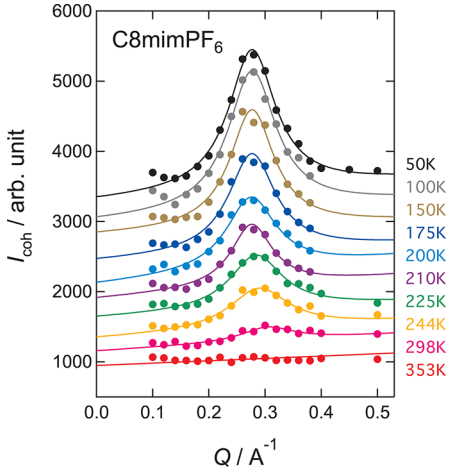

Figure 4. Neutron diffraction peaks at $Q \approx 0.3$ Å^{-1} for C8mimPF$_6$. Solid curves represent the results of the fit with Lorentz functions (see text for details). Data except at 353 K are shifted upward for clarity. Error bars are smaller than the symbols.

The parameters obtained from the fit are plotted in Figure 5. For both C8mimPF$_6$ and C8mimCl, in the heating direction, the peak position, Q_{low}, slightly shifts to the lower Q below the glass transition temperature, T_g (191 K for C8mimPF$_6$, 214 K for C8mimCl), but significantly shifts to the higher Q above T_g. Triolo et al. reported similar behavior in the X-ray diffraction measurement of C8mimBF$_4$ and interpreted the behavior as follows: the change of Q_{low} below T_g is due to the density change, while that above T_g relates to the diffusion of ions.[3] The Q_{low} corresponds to the distance between imidazolium rings separated by alkyl chains, as depicted in Figure 2b. The diffusion process and some local motions (such as alkyl-chain fluctuation) get activated above T_g, and then the alkyl chains are disordered (folded), leading to the shorter distance between imidazolium rings. This is analogous to the case of rubber elasticity above T_g driven by the entropic force. It is also possible that the alkyl chains interdigitate each other. As for the temperature dependence of the peak width, there is a tendency of increase in Γ above T_g. This tendency was also reported in the previous study on C8mimCl.[24]

The most interesting feature is that the peak intensity drastically increases upon cooling and does not saturate even below T_g. The intensity growth was already reported for C8mimBF$_4$[3] and C8mimCl,[24] but the change of the intensity below T_g was first observed in this work. It is unusual that the peak intensity varies below T_g where all configurational motions are frozen-in. This may indicate that the scattering intensity widely distributes in Q space. In other words, the correlation corresponding to the low-Q peak becomes stronger and

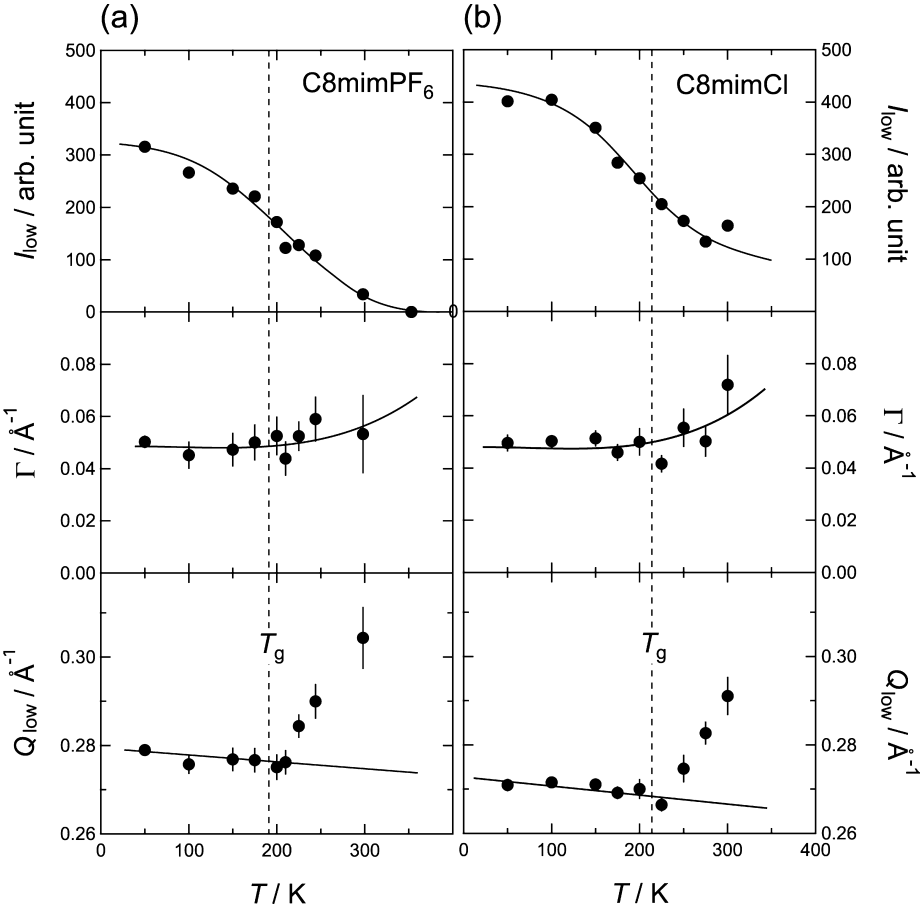

Figure 5. Temperature dependence of the integrated intensity I_{low}, the peak width Γ, and the peak position Q_{low} of the low-Q peak for (a) C8mimPF$_6$ and (b) C8mimCl. The vertical dashed line displays the glass transition temperatures, T_g's, where T_g = 191 K for C8mimPF$_6$[38] and T_g = 214 K for C8mimCl.[24] The solid lines are the guides to the eye.

dx.doi.org/10.1021/jp312608r | J. Phys. Chem. B 2013, 117, 2773−2781

develops even below T_g. Further studies under high Q resolution condition are required.

It was also found that there is a significant difference between $C8mimPF_6$ and C8mimCl; around T = 300 K, the intensity decreased to almost zero in $C8mimPF_6$, while the clear peak still exists in C8mimCl. This is linked to the fact that the relaxation at the low-Q peak was too slow to be detected in C8mimCl but could be observed in $C8mimPF_6$ as shown later. The temperature evolution of the structure in ILs is discussed later in combining with the QENS results.

Relaxation Related To the Ionic Correlation. We have carried out NSE measurements to investigate the relaxation processes at the nanostructure and ionic correlation peak positions (indicated by the arrows in Figure 2a). We first discuss the results on the ionic correlation peak. Figure 6 shows

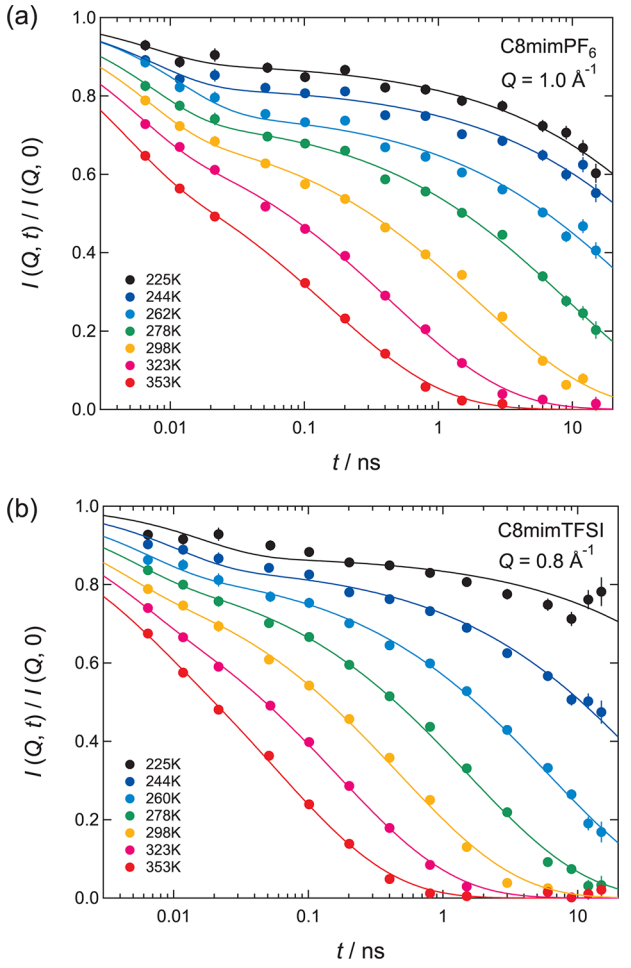

Figure 6. Intermediate scattering functions of (a) $C8mimPF_6$ observed at Q = 1.0 $Å^{-1}$ and (b) C8mimTFSI at Q = 0.8 $Å^{-1}$. Solid curves represent the results of the fit (see text for details).

the normalized intermediate scattering functions, $I(Q,t)/I(Q,0)$'s, of $C8mimPF_6$ at Q = 1.0 $Å^{-1}$ and C8mimTFSI at Q = 0.8 $Å^{-1}$. Two relaxation processes are supposed to reproduce the $I(Q,t)/I(Q,0)$'s for both samples, and the following function was used to fit the data:

$$I(Q,t)/I(Q,0) = f_1 \exp\left(-\frac{t}{\tau_1}\right) + f_2 \exp\left[-\left(\frac{t}{\tau_2}\right)^{\beta}\right] \quad (5)$$

where the first term is an exponential function corresponding to the faster relaxation, and the second one is a stretched exponential (Kohlrausch–Williams–Watts) function to the slower relaxation. The parameters f_1 and f_2 are the fractions of the faster and slower relaxations and should follow the constraint $f_1 + f_2 = 1$. τ_1 and τ_2 are the relaxation times, and β is the nonexponential parameter. We first fitted the data in the high temperature region ($T \geq 278$ K) treating β as a variable parameter. Next, the obtained values of β were ca. 0.5 in this temperature range. Hence, we fixed β to 0.5 in the final fitting, to obtain more reliable values for the relaxation times and the fractions. The results of the fit were quite good as shown in Figure 6.

The Arrhenius plot of the relaxation times and their fractions are displayed in Figure 7. The data of $C8mimCl^{24}$ are also

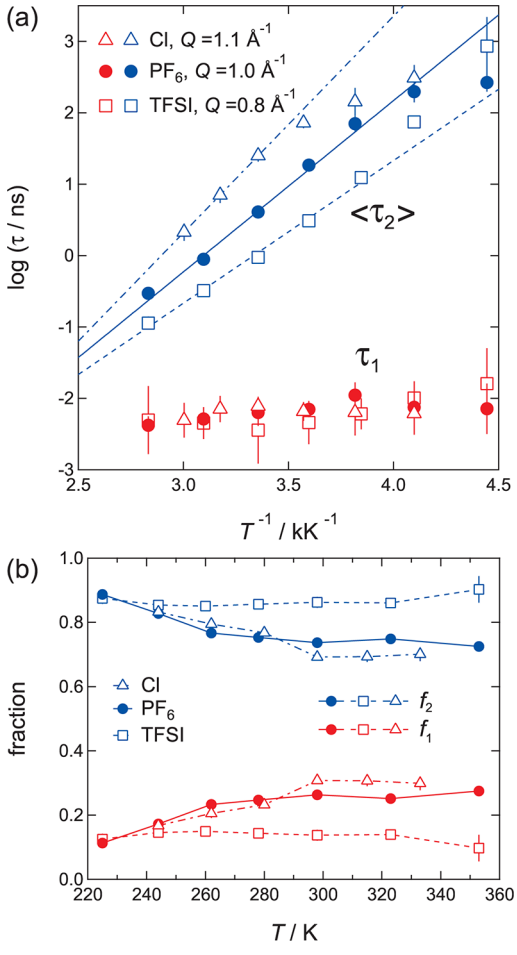

Figure 7. (a) Arrhenius plots of the relaxation times at Q = 1.0 $Å^{-1}$ (PF_6) and Q = 0.8 $Å^{-1}$ (TFSI). The data for $C8mimCl^{24}$ are also plotted for comparison. Two relaxation processes, faster one (τ_1) and slower one ($\langle\tau_2\rangle$), were observed at the Q positions. (b) Fractions of the relaxation, f_1 and f_2, as functions of temperature.

shown for comparison. Here, we plot the averaged relaxation times of τ_2 calculated from the equation $\langle\tau\rangle = \tau_{KWW}/\beta$. The faster relaxation time τ_1 does not exhibit a pronounced temperature dependence, indicating small activation energy (E_a). There is no difference in E_a between $C8mimPF_6$ and C8mimTFSI. On the other hand, the E_a's for $\langle\tau_2\rangle$ are relatively large and increase as the anion size decreases. The E_a's are estimated from the fitting with the Arrhenius equation $\tau = \tau_0$

dx.doi.org/10.1021/jp312608r | J. Phys. Chem. B 2013, 117, 2773–2781

$\exp(-E_a/k_BT)$, and the obtained values are E_a = 38.3 ± 1.6 kJ/mol (TFSI), 46.0 ± 2.6 kJ/mol (PF_6), and 58.1 ± 0.6 kJ/mol (Cl). The $\langle\tau_2\rangle$'s longer than 100 ns tend to deviate from the Arrhenius behavior as shown in Figure 7a. This often occurs and is because the measured Fourier time is limited up to 15 ns and the fit does not provide reliable values for the relaxation times longer than 100 ns.

As shown in Figure 7b, the fractions f_1 and f_2 do not change much with temperature, and f_2 is larger than f_1. Taking account of the temperature dependence of relaxation times and the fractions, we conclude that the slower relaxation (τ_2) corresponds to the relaxation of ionic correlation (ionic diffusion), while the faster one (τ_1) relates to local motions of the octyl-chain. It is known that the broad peak around Q = 1.5 $Å^{-1}$ in C8mimX results from the superimposition of many atomic correlations including an interalkyl-chain correlation. These correlations significantly contribute to the scattering intensity around Q = 1.0 $Å^{-1}$. The contribution for C8mimTFSI (measured at Q = 0.8 $Å^{-1}$) should be smaller than those for C8mimPF$_6$ (at Q = 1.0 $Å^{-1}$) and C8mimCl (at Q = 1.1 $Å^{-1}$). This is consistent with the fact that the f_1 of C8mimTFSI is smaller than those of C8mimPF$_6$ and C8mimCl. It is also reasonable that f_1 decreases as temperature decreases because the peak at Q = 1.5 $Å^{-1}$ shifts toward higher Q value on cooling.[2,11,12] In regard to the slower motion (τ_2), the E_a's strongly depend on anion, and this tendency is similar to that observed in the viscosity measurements.[25,26] Furthermore, the incoherent QENS study on C4mimPF$_6$[20] and the NSE work on d-C8mimCl[24] suggest that the ionic motion of ILs can be described by the KWW function with β of 0.5. The relative motion between the cations and anions, affected by long-range Coulomb interactions, exhibits more cooperative and nonexponential behavior.

Relaxation of the Low-Q Peak. Figure 8 presents the $I(Q,t)/I(Q,0)$ data collected at temperatures from 225 to 353 K for C8mimPF$_6$ and C8mimTFSI. Apparently, the $I(Q,t)/I(Q,0)$ curve does not follow a single relaxation behavior. The curves were fitted by three exponential functions as follows:

$$I(Q,t)/I(Q,0) = f_3 \exp\left(-\frac{t}{\tau_3}\right) + f_4 \exp\left(-\frac{t}{\tau_4}\right) + f_5 \exp\left(-\frac{t}{\tau_5}\right) \quad (6)$$

where f_3, f_4, and f_5 are the fractions of the relaxations with a constraint of $f_3 + f_4 + f_5 = 1$, and τ_3, τ_4, and τ_5 are the relaxation times. The relaxation times of the fastest motion, τ_3, are too fast to be determined by fitting the NSE data. Therefore, τ_3 was fixed to 0.004 ns to reproduce the 2 or 3 points with Fourier times shorter than 0.01 ns in the course of the fitting. As discussed later, two fast relaxation processes (τ_3 and τ_4) originate from the superimposition of several correlations, while the slower one (τ_5) is associated with the nanoscale structure. The former should be reproduced by many relaxation processes in principle, but we simply assume two exponential functions as a practical way in the analysis.

Figure 9 shows temperature dependences of the parameters obtained from the fit. The fastest motion, τ_3, is indicated by the thick line. The other motions, τ_4 and τ_5, are of Arrhenius-type, and the activation energy of τ_5 is higher than that of τ_4 for both C8mimPF$_6$ and C8mimTFSI. The deviation from the Arrhenius behavior for the longer relaxation times is due to

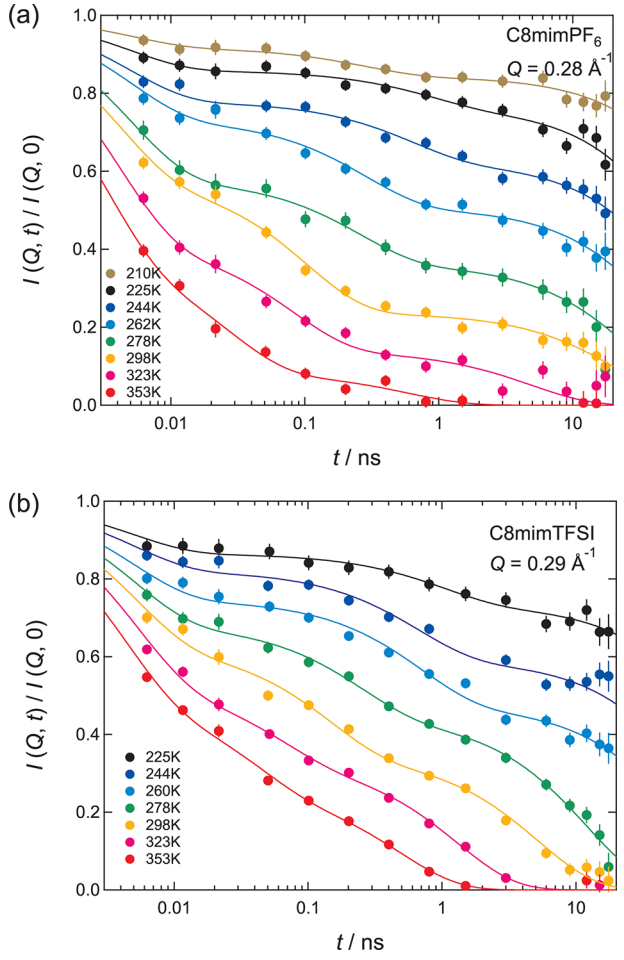

Figure 8. Intermediate scattering functions of (a) C8mimPF$_6$ observed at Q = 0.28 $Å^{-1}$ and (b) C8mimTFSI at Q = 0.29 $Å^{-1}$. Solid curves represent the results of the fit (see text for details).

the limitation of the Fourier time in this measurement, as is seen for the ionic diffusion discussed in the previous section (see Figure 7a). The estimated activation energies are 17.4 ± 1.6 kJ/mol (PF_6) and 22.0 ± 1.6 kJ/mol (TFSI) for the relaxation of τ_4 and 40.4 ± 7.7 kJ/mol (PF_6) and 36.5 ± 2.2 kJ/mol (TFSI) for that of τ_5.

The most important finding is the temperature dependence of the fractions. The fraction of the slowest motion, f_5, decreases with increasing temperature, while those of f_3 and f_4 tend to increase. This is in contrast to the fact the fractions f_1 and f_2 for the ionic correlation remain almost constant. This phenomenon suggests that there exists two states with inverse correlation in these ILs; upon heating, one associated with the slow relaxation decreases, while the other related to the fast relaxations increases.

To understand how the fraction of the two states evolves in temperature, we have to consider the fact that the low-Q peak becomes more intense on cooling. As described in the Experimental Section, $I(Q,t)$ is proportional to the echo amplitude divided by $I_{NSF} - I_{SF}$ (=C). The term C does not change much with temperature in most cases, but significantly changes at the low-Q peak in ILs. Hence, we show the temperature dependence of the fractions f_n multiplied by the factor C in Figure 10b. For comparison, the peak intensity I_{peak} and the nearly Q-independent coherent scattering I_0' are also plotted. Here, I_0' is I_0 (in eq 4) corrected for the effect of the

dx.doi.org/10.1021/jp312608r | J. Phys. Chem. B 2013, 117, 2773−2781

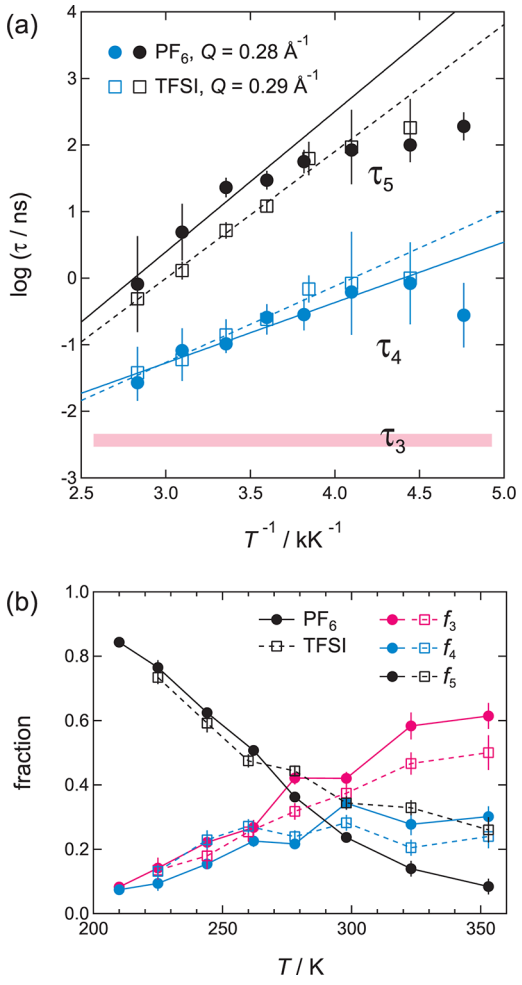

Figure 9. (a) Arrhenius plots of the relaxation times at $Q = 0.28$ Å^{-1} (PF_6) and $Q = 0.29$ Å^{-1} (TFSI). Three relaxation processes, τ_3, τ_4, and τ_5, were assumed to reproduce the $I(Q,t)/I(Q,0)$ data at these Q positions. The fastest one (τ_3) is too fast for the NSE measurements to evaluate the relaxation times. In the course of the fitting, τ_3 was fixed to ca. 0.004 ns that is indicated by the thick line in this figure. (b) Fractions of the relaxation processes, f_3, f_4, and f_5, as functions of temperature.

incoherent scattering. We evaluated I_0' ($=I_0 - I_{inc}/3$), according to the definition of the factor C:

$$C = I_{NSF} - I_{SF} = I_{coh} - \frac{1}{3}I_{inc} \quad (7)$$

In our samples, the intensity of the incoherent scattering is about one-half of that of the coherent scattering, so that the contribution from the incoherent scattering should be considered. The schematic explanation for I_{peak} and I_0' is given in Figure 10a.

The Cf_5 and I_{peak} drastically decrease with increasing temperature and exhibit similar temperature dependence. This suggests that the slow motion (τ_5) originates in the relaxation of the structure producing the low-Q peak. On the other hand, $C(f_3 + f_4)$ and I_0' tend to increase with temperature but do not lie on the same line. Because the sum of the scattering intensity is conserved, the decrease of I_{peak} gives rise to the slight increase of the scattering intensity in a wide Q region, which is consistent with the modest increase of I_0'. It is reasonable to expect that I_0' arises from the superimposition of several pair correlations, so that the fast motions (τ_3 and τ_4) are

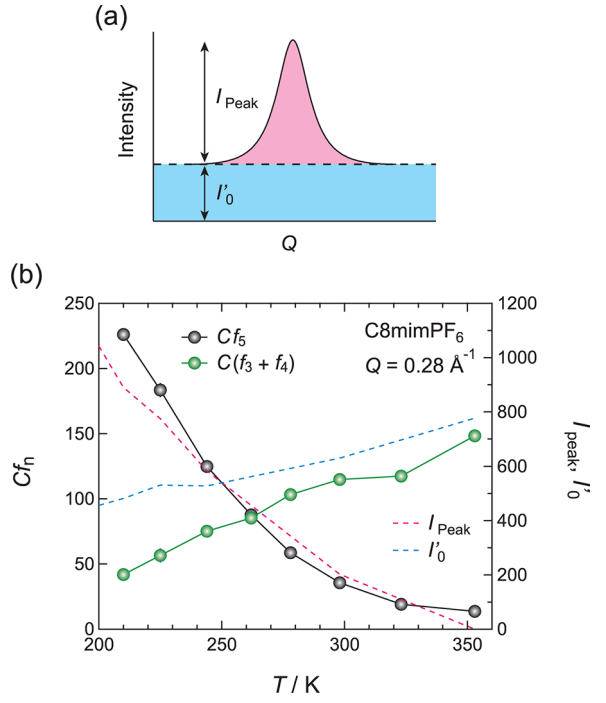

Figure 10. (a) Schematic drawing of I_{peak} and I_0'. (b) Temperature dependence of $C(f_3 + f_4)$ and Cf_5 for the left axis and I_{peak} and I_0' for the right axis. See the Experimental Section for details on C and I_0'.

associated with the relaxation related to some pair correlations separated by ~20 Å.

The present results have demonstrated that there exist two parts in ILs, one with the ordered nanoscale structure, the other with the disordered one. In other words, the structure and dynamics of ILs are spatially heterogeneous, and the fraction of each part changes with temperature. The ordered part becomes dominant at low temperature. At elevated temperatures, the ordered structure becomes smeared, and the disordered part increases. Considering the amphiphilicity (ionic imidazolium ring and neutral alkyl chain) in the cation, ILs can form several types of complex structure, such as micelle,[4] lamellar morphology, alkyl-group channel,[14] and so on. Figure 11 shows schematic drawings of possible ordered structures, lamellar and micelle-like structures. Both models have nanoscale domains of segregated neutral alkyl chains enclosed by a

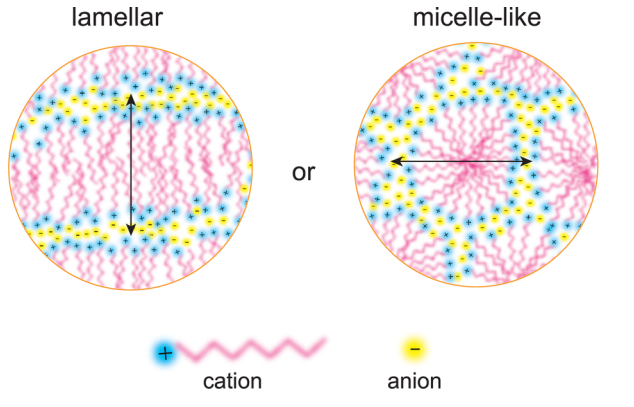

Figure 11. Schematic drawing of lamellar and micelle-like structure. The arrows correspond to the characteristic distance (~20 Å) of the low-Q peak.

dx.doi.org/10.1021/jp312608r | J. Phys. Chem. B 2013, 117, 2773−2781

charged network. The actual nanostructure may not be so rigid, and the boundary between the two parts may not be so clear. At elevated temperatures, there could be just pair correlation between ionic parts separated by alkyl chain as suggested by some structural studies.[6,8,9] At lower temperatures, however, we speculate that some sort of nanostructures, as shown in Figure 11, exist in ILs.

As compared to the micelle structure, the lamellar structure seems to be more realistic. It was suggested from the structural works that the crystal-like structure can exist in the liquid phase.[8,9] In fact, the crystal structure of ILs resembles the lamellar morphology, although there is a difference in the alkyl-chain interdigitation. Additionally, it was reported that the smectic liquid crystal phase really appears in ILs with longer alkyl chain ($n \geq 14$).[39] The precursor of smectic liquid crystal or short-range lamellar structure can be formed in C8mimX.

The activation energies (E_a's) of the slow relaxation of the nanostructure (τ_5) are comparable with those of ionic diffusion (τ_2), and the E_a becomes higher with a decrease in anion size. It implies that the slow relaxation related to the nanoscale structure is also mainly governed by the Coulomb interaction. The relaxation can be attributed to a fluctuation of the nanostructure, such as a layer-stretching motion in a lamellar structure and an expansion/contraction motion (breathing mode) in a micelle structure. The energy barrier for these types of motions is mainly due to the nearest-neighbor Coulomb interaction between ionic parts. It should noted that a kind of translational motion of polar/nonpolar domains themselves, which could have much higher E_a, does not occur.

To gain insights into the detailed structure in a nanometer scale, further structural studies, especially at low temperatures, are demanded. Furthermore, the correspondence between the fraction of the relaxation and the structural data would be confirmed by measuring partially deuterated samples in which the low-Q peak is enhanced.

CONCLUSION

To address the issues on the nanoscale structure in ILs, we have carried out neutron diffraction and neutron spin echo measurements for imidazolium-based ionic liquids C8mimX (X = Cl, PF_6, TFSI). All samples were fully deuterated to observe coherent scattering from ions. There were two distinct peaks at ca. 0.3 and 1.0 $Å^{-1}$. The higher-Q peak demonstrated that the interionic distance in C8mimPF_6 and C8mimTFSI becomes shorter with increasing temperature, but that in C8mimCl is insensitive to temperature, suggesting the stronger charge ordering in C8mimCl. However, the lower-Q peak, due to the nanoscale polar domains separated by neutral alkyl chains, becomes clearer (more ordered) on cooling and keeps growing even below T_g for both C8mimPF_6 and C8mimCl. In the higher temeprature region, the peak of C8mimPF_6 decreases to almost zero, but that of C8mimCl still remains, which is linked to the fact that the relaxation associated with the lower-Q peak in C8mimPF_6 is faster than that in C8mimCl.

In the relaxation study using NSE, we have observed the ionic diffusion and alkyl-chain dynamics at the position of ionic correlation ($Q_{ion} \approx 1.0$ $Å^{-1}$). The activation energy of the ionic diffusion increases with a decrease in anion size, which is analogous to the anion dependence of the viscosity, while E_a of alkyl relaxation is small and is hardly affected by the anions. As for the dynamics at the lower-Q peak position, two kinds of relaxation were found. It is of interest that the fraction of the slower relaxation increases upon cooling along with the growth of the lower-Q peak. The fraction of the faster motions, which are probably associated with the relaxation of several pair correlations with a distance of 20 Å, tends to increase with temperature. The above results implies the heterogeneity of structure and dynamics in ILs. The slower relaxation arises from the (ordered) nanoscale structure, while the faster ones are from the broken (disordered) part of the structure. As temperature decreases, the nanoscale structure becomes more ordered and dominant. This is the first experimental work investigating the motion related to the nanostructure in a wide temperature range. To make further discussion on the nanoscale structure, it is required to study the temperature dependence of the structure, more precisely, in conjunction with computer simulation studies.

AUTHOR INFORMATION

Corresponding Author

*E-mail: yamamuro@issp.u-tokyo.ac.jp.

Notes

The authors declare no competing financial interest.

ACKNOWLEDGMENTS

This work is financially supported by a Grant-in-Aid for Scientific Research on Priority Area no. 17073004, MEXT, Japan, and by the US-Japan Cooperative Program on Neutron Scattering. This work utilized facilities supported in part by the National Science Foundation under Agreement No. DMR-0944772.

REFERENCES

(1) Hardacre, C.; Holbrey, J. D.; McMath, S. E. J.; Bowron, D. T.; Soper, A. K. *J. Chem. Phys.* **2003**, *118*, 273−278.
(2) Triolo, A.; Mandanici, A.; Russina, O.; Rodrigues-Mora, V.; Cutroni, M.; Hardacre, C.; Nieuwenhuyzen, M.; Bleif, H.-J.; Keller, L.; Ramos, M. A. *J. Phys. Chem. B* **2006**, *110*, 21357−21364.
(3) Triolo, A.; Russina, O.; Bleif, H.-J.; Di Cola, E. *J. Phys. Chem. B* **2007**, *111*, 4641−4644.
(4) Triolo, A.; Russina, O.; Fazio, B.; Triolo, R.; Di Cola, E. *Chem. Phys. Lett.* **2008**, *457*, 362−365.
(5) Xiao, D.; Hines, L. G., Jr.; Li, S.; Bartsch, R. A.; Quitevis, E. L.; Russina, O.; Triolo, A. *J. Phys. Chem. B* **2009**, *113*, 6426−6433.
(6) Hardacre, C.; Holbrey, J. D.; Mullan, C. L.; Youngs, T. G. A.; Bowron, D. T. *J. Chem. Phys.* **2010**, *133*, 074510.
(7) Bodo, E.; Contrani, L.; Caminti, R.; Plechkova, N. V.; Seddon, K. R.; Triolo, A. *J. Phys. Chem. B* **2010**, *114*, 16398−16407.
(8) Annapureddy, H. V. R.; Kashyap, H. K.; De Biase, P. M.; Margulis, C. J. *J. Phys. Chem. B* **2010**, *114*, 16838−16846.
(9) Aoun, B.; Goldbach, A.; González, M. A.; Kohara, S.; Price, D. L.; Saboungi, M.-L. *J. Chem. Phys.* **2011**, *134*, 104509.
(10) Fujii, K.; Kanzaki, R.; Takamuku, T.; Kameda, Y.; Kohara, S.; Kanakubo, M.; Shibayama, M.; Ishiguro, S.; Umebayashi, Y. *J. Chem. Phys.* **2011**, *135*, 244502.
(11) Santos, C. S.; Annapureddy, H. V. R.; Murthy, N. S.; Kashyap, H. K.; Castner, E. W., Jr.; Margulis, C. J. *J. Chem. Phys.* **2011**, *134*, 064501.
(12) Santos, C. S.; Murthy, N. S.; Baker, G. A.; Castner, E. W., Jr. *J. Chem. Phys.* **2011**, *134*, 121101.
(13) Wang, Y.; Voth, G. A. *J. Am. Chem. Soc.* **2005**, *127*, 12192−12193.
(14) Lopes, J. N. A. C.; Costa Gomes, M. F.; Padua, A. A. H. *J. Phys. Chem. B* **2006**, *110*, 16816−16818.
(15) Noda, A.; Hayamizu, K.; Watanabe, M. *J. Phys. Chem. B* **2001**, *105*, 4603−4610.
(16) Tokuda, H.; Hayamizu, K.; Ishii, K.; Susan, M. A. B. H.; Watanabe, M. *J. Phys. Chem. B* **2004**, *108*, 16593−16600.

(17) Antony, J. H.; Dölle, A.; Mertens, D.; Wasserscheid, P.; Carper, W. R.; Wahlbeck, P. G. *J. Phys. Chem. A* **2005**, *109*, 6676−6686.
(18) Sangoro, J. R.; Iacob, C.; Naumov, S.; Valiullin, R.; Rexhausen, H.; Hunger, J.; Buchner, R.; Strehmel, V.; Kärger, J.; Kremer, F. *Soft Matter* **2011**, *7*, 1678−1681.
(19) Endo, T.; Widgeon, S.; Yu, P.; Sen, S.; Nishikawa, K. *Phys. Rev. B* **2012**, *85*, 054307.
(20) Triolo, A.; Russina, O.; Arrighi, V.; Juranyi, F.; Janssen, S.; Gordon, C. M. *J. Chem. Phys.* **2003**, *119*, 8549−8557.
(21) Triolo, A.; Russina, O.; Hardacre, C.; Nieuwenhuyzen, M.; Gonzalez, M. A.; Grimm, H. *J. Phys. Chem. B* **2005**, *109*, 22061−22066.
(22) Inamura, Y.; Yamamuro, O.; Hayashi, S.; Hamaguchi, H. *Physica B* **2006**, *385*−*386*, 732−734.
(23) Russina, O.; Beiner, M.; Pappas, C.; Russina, M.; Arrighi, V.; Unruh, T.; Mullan, C. L.; Hardacre, C.; Triolo, A. *J. Phys. Chem. B* **2009**, *113*, 8469−8474.
(24) Yamamuro, O.; Yamada, T.; Kofu, M.; Nakakoshi, M.; Nagao, M. *J. Chem. Phys.* **2011**, *135*, 054508.
(25) Seddon, K. R.; Stark, A.; Torres, M.-J. In *Clean Solvents: Alternative Media for Chemical Reactions and Processing*; Abraham, M. A., Moens, L., Eds.; ACS Symposium Series; American Chemical Society: Washington, DC, 2002; Chapter 4.
(26) Tokuda, H.; Tsuzuki, S.; Susan, M. A. B. H.; Hayamizu, K.; Watanabe, M. *J. Phys. Chem. B* **2006**, *110*, 19593−19600.
(27) Yu, G.; Zhao, D.; Wen, L.; Yang, S.; Chen, X. *AIChE J.* **2012**, *58*, 2885−2899.
(28) Daguenet, C.; Dyson, P. G.; Krossing, I.; Oleinikova, A.; Slattery, J.; Wakai, C.; Weingärtner, H. *J. Phys. Chem. B* **2006**, *110*, 12682−12688.
(29) Nakamura, K.; Shikata, T. *ChemPhysChem* **2010**, *11*, 285−294.
(30) Sangoro, J. R.; Mierzwa, M.; Iacob, C.; Paluch, M.; Kremer, F. *RSC Adv.* **2012**, *2*, 5047−5050.
(31) Widegren, J. A.; Saurer, E. M.; Marsh, K. N.; Magee, J. W. *J. Chem. Thermodyn.* **2005**, *37*, 569−575.
(32) Zech, O.; Stoppa, A.; Buchner, R.; Kunz, W. *J. Chem. Eng. Data* **2012**, *55*, 1774−1778.
(33) Kofu, M.; Someya, T.; Tatsumi, S.; Ueno, K.; Ueki, T.; Watanabe, M.; Matsunaga, T.; Shibayama, M.; Sakai, V. G.; Tyagi, M.; Yamamuro, O. *Soft Matter* **2012**, *8*, 7888−7897.
(34) Fujii, K.; Ueki, T.; Niitsuma, K.; Matsunaga, T.; Watanabe, M.; Shibayama, M. *Polymer* **2011**, *52*, 1589−1595.
(35) Rosov, N.; Rathgeber, S.; Monkenbusch, M. In *Scattering from Polymers: Characterization by X-rays, Neutrons, and Light*; Cebe, P., Hsaio, B. S., Lohse, D. J., Eds.; ACS Symposium Series; American Chemical Society: Washington, DC, 2000; Chapter 7.
(36) Monkenbusch, M.; Schätzler, R.; Richter, D. *Nucl. Instrum. Methods Phys. Res., Sect. A* **1997**, *399*, 301−323.
(37) Azuah, R. T.; Kneller, L. R.; Qiu, Y.; Tregenna-Piggott, P. L. W.; Brown, C. M.; Copley, J. R. D.; Dimeo, R. M. *J. Res. Natl. Inst. Stand. Technol.* **2009**, *114*, 341.
(38) Huddleston, J. G.; Visser, A. E.; Reichert, W. M.; Willauer, H. D.; Broker, G. A.; Rogers, R. D. *Green Chem.* **2001**, *3*, 156−164.
(39) Gordon, C. M.; Holbrey, J. D.; Kennedy, A. R.; Seddon, K. R. *J. Mater. Chem.* **1998**, *8*, 2627−2636.